Stability and Folding Kinetics of Structurally Characterized Cytochrome *c*-b_{562}[†,‡]

Jasmin Faraone-Mennella,[§] F. Akif Tezcan,[§] Harry B. Gray,* and Jay R. Winkler*

Beckman Institute, California Institute of Technology, 1200 East California Boulevard, Pasadena, California 91125

Received February 5, 2006; Revised Manuscript Received April 24, 2006

ABSTRACT: The four-helix-bundle protein fold can be constructed from a wide variety of primary amino acid sequences. Proteins with this structure are excellent candidates for investigations of the relationship between folding mechanism and topology. The folding of cytochrome b_{562}, a four-helix-bundle heme protein, is hampered by heme dissociation. To overcome this complication, we have engineered a variant of cytochrome b_{562} (cyt *c*-b_{562}) featuring a *c*-type linkage between the heme and the polypeptide chain. The replacement of the native cyt b_{562} leader sequence in this protein with that of a *c*-type cytochrome (cyt c_{556}) led to high yields of fully matured and correctly folded cyt *c*-b_{562}. We have determined the X-ray crystal structure of cyt *c*-b_{562} at 2.25 Å and characterized its physical, chemical, and folding properties. These measurements reveal that the *c*-type linkage does not perturb the protein fold or reduction potential of the heme group. The covalent attachment of the porphyrin to the polypeptide does, however, produce a substantial change in protein stability and folding kinetics.

Both experimental and theoretical work suggests a strong correlation between topology and folding time for small monomeric proteins (*1*−*4*). The topology of a protein fold can be characterized by its contact order, a measure of the average number of residues separating secondary and tertiary contact sites (*1*). Inasmuch as the topology of a protein is largely defined by the conformation of the polypeptide backbone, contact-order models point to a relatively minor role for primary amino acid sequence in determining folding kinetics. Nevertheless, there are examples of topologically similar proteins that exhibit widely divergent folding time scales, suggesting that the amino acid sequence can be a determinant of folding dynamics (*2*−*5*).

Four-helix-bundle proteins provide an excellent opportunity to address the folding-topology riddle, since they exhibit a strongly conserved structural motif with wide variations in primary amino acid sequence and, in some cases, folding times that approach the time scale accessible by computer simulations. Four-helix bundles are found in numerous evolutionarily unrelated proteins, such as interleukin-2 (*6*), apolipoprotein (*7*), human growth hormone (*8*), and *Helicobacter pylori* neutrophil activating protein (*9*). These proteins perform a diverse array of functions, ranging from RNA binding to polysaccharide cleavage in T4 lysozyme and electron transfer in cytochrome (cyt)[1] b_{562}.

Our interest has focused on a family of four-helix-bundle cytochromes that displays substantial variations in folding behavior. For instance, electron-transfer-triggered folding of Fe^{2+}-cyt b_{562} has been found to yield folded protein on a submillisecond time scale, whereas cyt *c*′ requires several seconds to fold completely (*10*−*12*). Part of this difference can be ascribed to differences in the porphyrin−polypeptide linkage (*10, 13*). Four-helix-bundle cytochromes contain one or more heme (Fe−protoporphyrin IX) groups, and their structural topology is almost perfectly conserved (≈3 Å rmsd) (*14*−*16*), despite variation in the attachment and coordination of the heme group. In the *b*-type cytochromes (e.g., cyt b_{562}), the heme is attached to the polypeptide only through axial Fe ligation, whereas in the case of the *c*-type cytochromes, the α-carbons of the protoporphyrin vinyl groups form thioether linkages to the two cysteines found in a strongly conserved CXXCH motif (e.g., cyt *c*′, cyt c_{556}). The evolutionary advantages arising from covalent attachment of the heme to the polypeptide chain have not been clearly elucidated (*17*), and the question whether the different cytochrome heme linkages are the consequence of convergent or divergent evolution remains open (*17*).

In the case of cyt b_{562}, featuring a noncovalently bound protoporphyrin, we found that the kinetics of heme dissociation from the polypeptide [$k_{diss} \approx (2-7) \times 10^3\ s^{-1}$] compete with refolding dynamics, limiting the yield of the folding reaction in the reduced state and causing irreversible unfolding in the oxidized state; and, at the time, we recognized that slower folding populations in the unfolded ensemble of cyt b_{562} would not be detected because of heme dissociation (*10*). Indeed, it has been reported that under denaturing conditions some cyt b_{562} remains in a near-native conformation and that the proportion of this conformation correlates well with the fraction of protein that successfully refolds (*13*). To eliminate problems with heme dissociation in cyt b_{562} refolding, we set out to prepare a variant of cyt b_{562} (*c*-b_{562})

† This work was supported by National Institutes of Health Grant GM068461 (J.R.W.) and the Ellison Medical Foundation (Senior Scholar Award in Aging to H.B.G.).

‡ Atomic coordinates and structure factors for cytochrome *c*-b_{562} have been deposited in the Protein Data Bank (PDB ID code 2BC5).

* To whom correspondence should be sent. E-mail: hbgray@caltech.edu; winklerj@caltech.edu. Tel: 626-395-6500; 626-395-2834. Fax: 626-449-4159.

§ Current address: Department of Chemistry and Biochemistry, University of California, San Diego, 9500 Gilman Drive, MC 0332, La Jolla, CA 92093-0332.

[1] Abbreviations: cyt, cytochrome; GuHCl, guanidine hydrochloride.

10.1021/bi060242x CCC: $33.50
Published on Web 08/10/2006

with the protoporphyrin cofactor covalently linked to the polypeptide chain.

Barker and co-workers first reported the conversion of cyt b_{562} to a *c*-type cytochrome (*18*). In this work, single Cys mutations at positions 98 (R98C) and 101 (Y101C), as well as a double mutation (R98C/Y101C), were introduced into the cyt b_{562} polypeptide sequence. Holoproteins with *c*-type thioether linkages between the protoporphyrin were isolated with all three mutant proteins. The yield of holoprotein with the R98C mutant was reported to be comparable to that of wild-type cyt b_{562}, but holoprotein production with either the Y101C mutant or the R98C/Y101C double mutant was substantially reduced. Nevertheless, a fraction of the holoprotein isolated with the R98C/Y101C double mutant sequence appeared to have two *c*-type thioether linkages. Barker noted that constructs with the R98C mutation would produce blue-green-colored protein if periplasmic extracts were not kept under anaerobic conditions (*18*), and he later reported the isolation of a biliverdin-containing construct of cyt b_{562} with a covalently attached heme (*19*). Structural characterization of the R98C mutant by NMR spectroscopy confirmed the presence of the single *c*-type thioether linkage (*18*, *20*). Chemical denaturation studies of the R98C holoprotein revealed a 5.6 kJ mol^{-1} increase in folding stability relative to wild-type cyt b_{562} (*20*). In an effort to improve the yield of cyt b_{562} with two *c*-type thioether linkages, a new expression system was developed which incorporated the plasmid for the cytochrome *c* maturation (Ccm) system (*21*−*23*). This approach led to increased homogeneity of holoprotein with two *c*-type thioether linkages, although the yield of isolated protein did not increase over that obtained in the absence of the Ccm system (0.3−1.8 mg/g of wet cells) (*22*).

Using the cyt b_{562} plasmid available in our laboratory [pNS207b562 (*24*)], the cytochrome *c* maturation gene cassette [pEC86 (*21*)], and a commercially available *Escherichia coli* strain [BL21(DE3)], we were not able to prepare holoprotein with two *c*-type thioether linkages, isolating instead green-colored proteins suggesting heme oxidation (*19*). Subsequently, we developed a protocol that has enabled us to overexpress c-b_{562} reproducibly and in high yield. In this paper we provide experimental details of our cyt c-b_{562} expression system, as well as the X-ray crystal structure (2.25 Å resolution) and physical, chemical, and folding properties of this protein. We find that the presence of two *c*-type thioether linkages does not substantially perturb the wild-type fold but, like the R98C mutant with one *c*-type thioether linkage (*20*), does have a substantial impact on protein folding stability. We also report the folding kinetics of Fe^{3+}-cyt c-b_{562} and compare them to those of Fe^{2+}-cyt c-b_{562} (*25*) as well as other four-helix-bundle heme proteins.

MATERIALS AND METHODS

Bacterial Strains and Plasmid. E. coli strain XL1-blue from Stratagene was used for the ligation and sequencing steps. *E. coli* BL21(DE3) from Novagen was used for protein expression.

The plasmid carrying the complete *E. coli* cyt b_{562} gene, pNS207b562, was kindly provided by S. G. Sligar (*24*). The plasmid encoding the complete gene for cyt c_{556}, pETc556, was available in our laboratory (*26*). The cytochrome *c* maturation gene cassette (*ccm* or pEC86) was provided by L. Thöny-Meyer (*21*).

Molecular Genetics. Oligonucleotides were obtained from Invitrogen. PCR was performed using a QuickChange mutagenesis kit. Amersham Biosciences DNA purification kits were used to purify PCR products and to isolate restriction fragments from agarose gels. DNA sequencing was performed by the Caltech DNA Sequencing Core Facility.

Chimeric Gene Encoding Engineered Cyt c-b_{562}. A chimeric gene was constructed by ligating a fragment of *Rhodopseudomonas palustris* cyt c_{556} encoding the N-terminal signal sequence in-frame to an engineered fragment of *E. coli* cyt b_{562} encoding the R98C/Y101C cyt b_{562} mutant (c-b_{562}) necessary for *c*-type linkage of the heme group to the polypeptide chain through two thioether bonds.

A foreign restriction site, *BSTE*II, was introduced by site-directed mutagenesis into pETc556, located after the N-signal peptide encoding region. The plasmid was then linearized with *BSTE*II and *Nde*I restriction enzymes to excise the region encoding mature cyt c_{556} (pETc-).

The coding sequence (without leader) of mature cyt b_{562} was lifted by PCR from the original construct (pNS207b562). Primers 1 and 2 were used to introduce 5′ *Nde*I and 3′ *BSTE*II sites, which introduce the A1V/D2T mutations in the first two residues of the mature cyt b_{562} sequence. The PCR product was then restricted with *Nde*I and *BSTE*II and subsequently cloned into the pETc- vector carrying the leader sequence from cyt c_{556}. The unique *BSTE*II site was then removed, reverting the A1V/D2T mutation, and a tryptophan residue (Y59W) was introduced (for use as a fluorescent probe) by site-directed mutagenesis. We denote the plasmid thus obtained as pETc-b562.

Protein Expression. Plasmid (pETc-b562) was cotransformed with pEC86 in *E. coli* strain BL21(DE3). Transformants were initially grown overnight on LB agar plates containing ampicillin (60 μg/mL) and chloramphenicol (34 μg/mL). Approximately 4 in 10 colonies were visibly red, indicating cytochrome overexpression. After inoculation in LB medium, cells were subjected to rotary shaking at 110 rpm at 37 °C and grown overnight. Cells were harvested after the cell density reached an OD_{600} of ∼1.8. No induction was necessary.

Protein Purification and Characterization. Cyt c-b_{562} was purified by ion-exchange chromatography on a Q-Sepharose Fast Flow column, followed by a second purification step on a Mono S column (Pharmacia FPLC). The purity of protein samples was assessed by SDS−PAGE gel electrophoresis and by mass spectroscopy. Electrospray mass spectroscopy and N-terminal amino acid sequencing were performed by the Protein/Peptide Microanalytical Laboratory in the Beckman Institute.

Equilibrium Unfolding. Guanidine hydrochloride (GuHCl, ultrapure grade; Sigma) was used as received. Circular dichroism (CD) and fluorescence spectra were recorded using an Aviv 62ADS spectropolarimeter and a Jobin Yvon SPEX Fluorolog-3 spectrofluorometer (λ_{ex} 290 nm; λ_{em} 300−500 nm), respectively. Steady-state absorption spectra were measured on HP-8453 and HP-8452 diode array spectrometers. GuHCl concentrations in the samples were determined from refractive indices measured on an Abbe-3L refractometer (Milton Roy, Rochester, NY) (*27*).

Folding Kinetics. The refolding kinetics of Fe^{3+}-cyt *c*-b_{562} were measured using a BioLogic SFM-4S stopped-flow mixer coupled via an optical fiber to a 200 W mercury/xenon arc lamp excitation source. For absorbance-monitored folding kinetics measurements, transmitted probe light was directed by the optical fiber through a monochromator to a nine-stage photomultiplier tube (Hamamatsu R928); observation wavelengths were 398 and 418 nm. For fluorescence-probed folding kinetics, the excitation source was filtered ($260 \leq \lambda_{ex} \leq 300$ nm), and the fluorescence was detected with the monochromator set to 354 nm. Kinetics traces were collected for time periods up to 3 s, typically at a sampling rate of 20 kS/s.

For refolding experiments, a stock of unfolded cyt *c*-b_{562} (100−200 μM in 7 M GuHCl, pH 5) was diluted with a combination of 100 mM sodium acetate and a 7 M GuHCl solution at pH 5, resulting in final protein concentrations of 7−10 μM and varying GuHCl concentrations (0.3−2 M). The stopped-flow mixing dead time under these conditions was ∼5 ms. Kinetics traces were fitted using Igor4Pro or Matlab.

Fluorescence Energy Transfer Kinetics. Tryptophan fluorescence decay kinetics measurements were carried out as previously described (*12*, *28*). Protein samples (3−5 μM unless otherwise stated) were deoxygenated by repeated evacuation/Ar-fill cycles on a Schlenk line. A polarized laser pulse (35° from vertical) from the third harmonic (290 nm) of a regeneratively amplified femtosecond Ti:sapphire laser (Spectra-Physics) was used as an excitation source, and a picosecond streak camera (Hamamatsu C5680) was used in the photon-counting mode for detection. Tryptophan emission was selected by an interference filter ($\lambda = 355 \pm 5$ nm). Trp luminescence decay kinetics were modeled with the function $I(t) = I_0(t) \int P(r) \exp(-k_{et}(r)t)\, dr$, where $I_0(t)$ is the Trp fluorescence decay in the absence of energy transfer to the heme, $P(r)$ is the probability of observing a conformation with donor−acceptor distance r, and $k_{et}(r)$ is the rate of energy transfer at distance r. Distance distributions were extracted from the decay kinetics by numerical inversion of the Laplace transform describing $I(t)$. The critical constraint for this inversion is the requirement that $P(r) \geq 0$. A linear least squares MATLAB (Mathworks, Natick, MA) algorithm with a nonnegativity constraint (LSQNONNEG) was used to project the narrowest $P(k)$ distributions from the fluorescence kinetics. A transformation using the Förster equation recasts the $P(k)$ distributions obtained by LSQNONNEG into distributions over r (*29*) [$k(r) = k_o(R_o/r)^{1/6}$, where k_o is the excited-state decay rate constant of excited *N*-acetyltryptophanamide and R_o is the critical Förster distance for Trp−heme energy transfer]. The value of R_o for orientationally averaged Trp−heme FET is 34 Å (*12*); the experimental limit for distances extracted from this analysis is ∼50 Å. In folded cyt *c*-b_{562}, the Trp side chain is likely to be locked into a configuration that prevents orientatonal averaging faster than the decay of singlet-excited Trp. Using the Fe-cyt *c*-b_{562} X-ray crystal structure coordinates, and previously determined transition moment orientations (*30*), we estimate that R_o for this Trp−heme configuration is 38 Å.

X-ray Crystallography. Crystals of cyt *c*-b_{562} were grown by vapor diffusion in sitting drops. The reservoir solution was 500 μL of 70% $(NH_4)_2SO_4$ (pH 5). The crystallization drop was prepared by mixing 2 μL of 1 mM cyt *c*-b_{562} (5 mM sodium acetate, 20 mM NaCl, pH 5) with 2 μL of the reservoir solution. Crystals ($P2_12_12_1$, 63.861 Å × 68.158 Å × 90.440 Å) typically appeared within 1 day and were grown for at least a week until they reached a size of 200 × 200 × 100 μm. X-ray diffraction data were collected at 100 K using an R-Axis IV imaging plate area detector and monochromatized Cu−Kα radiation (1.54 Å) produced by a Rigaku RU 200 rotating anode generator operated at 50 kV and 100 mA. The data were processed using DENZO and SCALEPACK (*31*) (overall $R_{sym} = 7.9\%$, overall $I/\sigma I = 13.3$, redundancy = 3.4, completeness = 98.7%). The structure of cyt *c*-b_{562} was determined at 2.25 Å by molecular replacement with MOLREP (*32*) using the wild-type cyt b_{562} structure (PDB ID code 256B) (*33*) as the search model. Rigid-body, simulated annealing, positional, and thermal refinement with CNS (*34*), along with manual rebuilding, and water placement with XFIT (*35*), produced the final model ($R_{cryst} = 23.3\%$, $R_{free} = 27.7\%$, overall *B*-factor = 24.6 Å^2). The Ramachandran plot calculated with PROCHECK (*36*) indicates 96.9% of the residues to be in the most favored, 2.8% to be in the allowed, and 0.3% to be in the generously allowed regions. Atomic coordinates and structure factors for cyt *c*-b_{562} have been deposited in the Protein Data Bank (PDB ID code 2BC5).

RESULTS AND DISCUSSION

Protein Expression. The biosynthesis of *c*-type cytochromes has been achieved aerobically in *E. coli* by coexpressing the cytochrome with the cyt *c* maturation gene cassette (*ccm*) developed by Thöny-Meyer and co-workers (*21*) or using heme lyase as first described by Mauk (*37*−*39*). Although heroic efforts have been made in recent years to elucidate these biosynthetic mechanisms (*40*, *41*), it is still not clear in atomic detail just how the *ccm* proteins and heme lyase form the *c*-type linkage in cytochromes.

Initial attempts to form the mature *c*-type linkage in b_{562} were carried out by inserting the conserved CXXCH heme binding motif by site-directed mutagenesis into wild-type cyt b_{562}. As a start, the pNS207 plasmid harboring the DNA sequence encoding the engineered R98C/Y101C cyt b_{562} was cotransformed with the pEC86 plasmid carrying the *ccm*A−H maturation genes in *E. coli* BL21(DE3) cells. Transformants were initially grown overnight on LB agar plates containing ampicillin and chloramphenicol. After inoculation in LB and incubation at 37 °C for ca. 6 h, all colonies produced red pellets, indicating heme protein overproduction. Yet, the periplasmic protein obtained by osmotic shock proved to be unstable, turning green upon prolonged exposure to air. Similar behavior, indicative of heme oxidation, has been reported previously (*18*, *19*). Guanidine or acid treatment resulted in loss of the heme group, and electrospray mass spectroscopy revealed the apoprotein as the sole product, signaling the absence of covalent porphyrin attachment. Thus, we were not able to express the holoprotein by simply mutating the DNA sequence encoding for R98C/Y101C/b_{562} and coexpressing it with pEC86 in *E. coli* BL21(DE3). This approach, however, has been successful in other laboratories using a different cyt b_{562} plasmid and *E. coli* strain (*18*, *22*, *23*).

Several studies have highlighted the necessity of an appropriate N-signal peptide to target the gene product to the periplasm where maturation of cytochromes *c* takes place

(*42*, *43*); the information stored in the N-signal peptide can be responsible for "errors" during the maturation of *c*-type proteins. We therefore reasoned that replacing the signal sequence of cyt b_{562} with that of a *c*-type cytochrome might lead to successful overexpression of cyt c-b_{562}.

To this end, we combined the DNA sequence of cyt b_{562} with the leader sequence signaling for cyt c_{556}, for which a successful expression system was already available (*26*). The chimera thus obtained (pETc-b562) was cotransformed with pEC86 in *E. coli* BL21(DE3). Approximately 10 mg of highly purified recombinant c-b_{562} was obtained from 1 L of cell culture in LB. The periplasmic protein isolated from the cell by osmotic shock was shown by mass spectrometry to correspond to the mature holoprotein (12341 amu). No apoprotein was detected in the cell extract. N-terminal sequence analysis yielded Ala-Asp-Leu-Glu as the first four residues of the mature protein. Interestingly, expression of recombinant c-b_{562} protein lacking the Trp59 mutation (i.e., with the wild-type Lys59 residue) resulted in some protein with oxidized (green) heme groups along with correctly folded protein.

Structural and Physical Characterization. The X-ray structure of cyt c-b_{562} was solved at 2.25 Å resolution using crystals obtained from 70% ammonium sulfate at pH 5 (Figure 1a). The asymmetric unit of the orthorhombic cyt c-b_{562} crystals contains four nearly identical molecules which are associated in pairs. This lattice arrangement is quite distinct from that observed for the triclinic wild-type cyt b_{562} crystals (PDB ID code B256) that were obtained under similar crystallization conditions (*33*). The pairing of cyt c-b_{562} molecules is largely mediated by an extensive interface (buried surface area = 775 Å^2) formed by the antiparallel alignment of residues 55−83, leading to pairwise interactions between helix side chains. This arrangement leads, among other polar interactions, to close contacts between Asp66 and Asp73 that would be expected to be destabilizing. The interface also features hydrophobic interactions between the highly exposed side chains of Leu76 and Trp59 ($d \approx 4.0$ Å), the latter engineered in place of a lysine for fluorescence studies. Under the high-ionic-strength crystallization conditions, this hydrophobic interaction is apparently strong enough to negate the destabilizing effect of Asp−Asp pairing and yield a crystal lattice that is quite disparate from that of wild-type cyt b_{562}. In addition, the Trp59 indole interacts with the guanidinium group of Arg62 ($d \approx 3.1$ Å, Figure 1a). Such π−cation interactions have been calculated to be stabilizing by up to 23 kJ mol^{-1} (*44*), although model systems based on helical peptides show this effect to be a more modest 1.7−8.4 kJ mol^{-1} (*45*, *46*). The Trp59−Arg62 interaction could nevertheless contribute to the improved expression of this c-b_{562} variant over its pseudo-wild-type counterpart, which contains a Lys in the 59 position (vide infra).

Cyt c-b_{562} electron density maps clearly demonstrate the presence of thioether linkages between Cys98 and Cys101 and the heme group (Figure 1b) (average bond distance = 1.83 Å); these maps also show that the heme environment and the Fe coordination are not significantly perturbed from those in the wild-type protein (Figure 2b). The average rmsd in C_α positions between cyt c-b_{562} and wild-type cyt b_{562} is 0.42 Å, ranging from 0.9 Å for residues in the loops connecting the first and second, as well as the second and third helices, to 0.2 Å for residues within the helical regions (Figure 2a). As expected from the differences in amino acid sequence and porphyrin−peptide bonding, structural variations between cyt c-b_{562}, wild-type cyt b_{562} (*33*), and the R98C mutant with a single *c*-type thioether linkage (*20*) are apparent in the vicinity of the heme. In particular, the plane of the His102 imidazole ring in cyt c-b_{562} is rotated ~17° from its position in the wild-type protein and approximately 30° from its position in the R98C mutant (*20*).

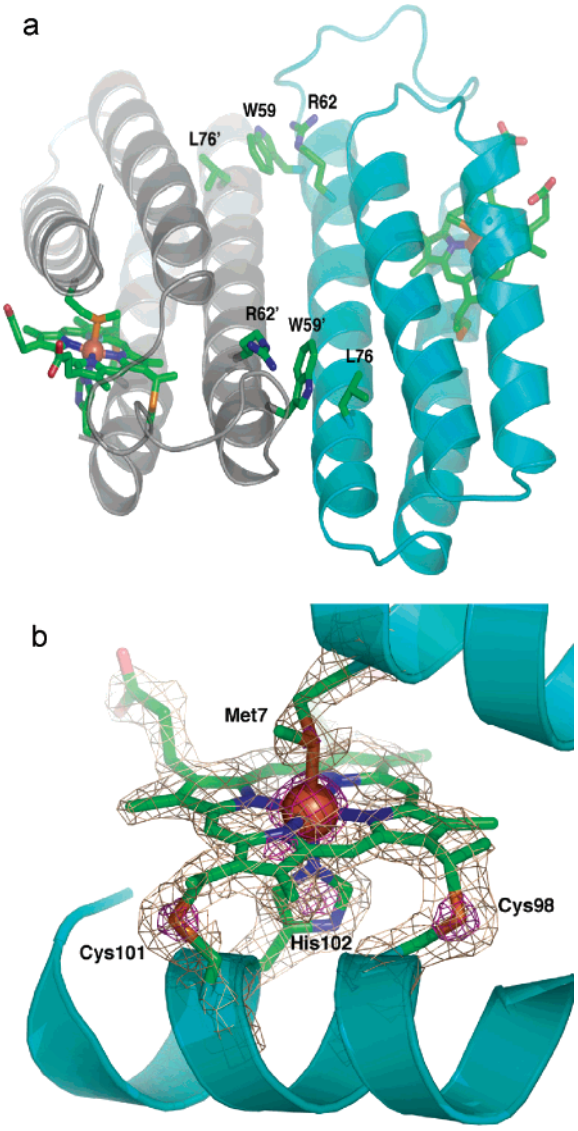

FIGURE 1: Structural details from the 2.25 Å crystal structure of cyt c-b_{562}. (a) Backbone ribbon showing one of the two dimers in the asymmetric unit. Monomers are colored gray and cyan, respectively. The dimer interface involves largely the third helices, aligned in an antiparallel fashion; the interfacial contacts include the pairwise hydrophobic interaction between the Trp59 and Leu76 side chains. The Trp59−heme FET pair center-to-center distance is ~19 Å. (b) $2F_o - F_c$ electron density map of the heme environment (wheat, 1.5σ; purple, 4σ) showing the *c*-type linkages between the heme periphery and the engineered Cys98 and Cys101 located on the C-terminal helix.

The absorption spectrum of cyt c-b_{562} is consistent with the introduction of a *c*-type heme: the Soret and the Q_{00} maxima for the Fe^{3+} (415 and 527 nm) and Fe^{2+} proteins (421 and 556 nm) are quite similar to those in cyt c_{556} (Figure 3) (*25*). Extinction coefficients for Soret bands were determined using the pyridine hemochrome method (*47*):

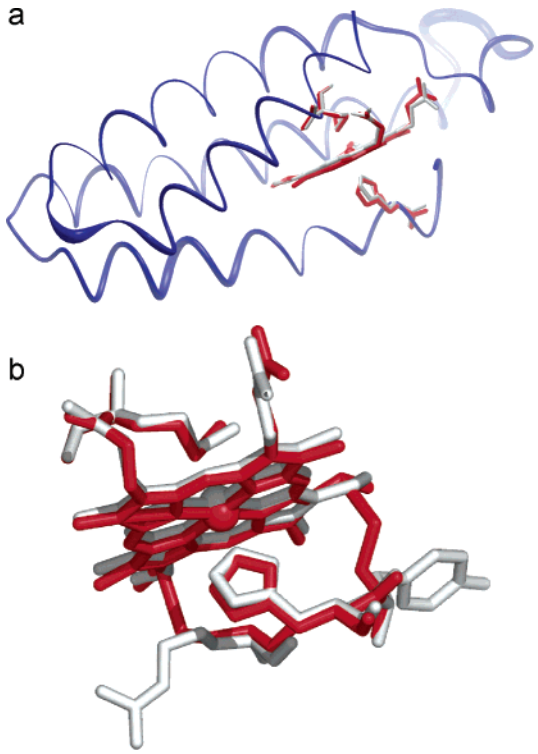

FIGURE 2: Comparison of the structures of wild-type cyt b_{562} and *c*-b_{562}. (a) Superposition of the structures where the diameter of the tube is proportional to the root-mean-square deviation (rmsd) between the two. (b) Comparison of the structures in the vicinity of the heme of wild-type cyt b_{562} (gray) and cyt *c*-b_{562} (red).

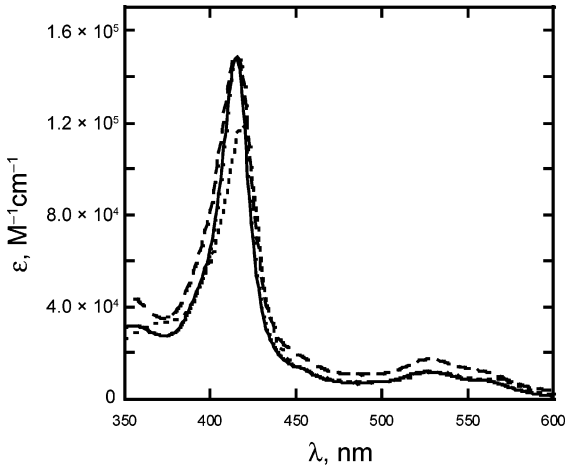

FIGURE 3: Absorption spectra of four-helix-bundle heme proteins (pH 7): wild-type Fe^{3+}-cyt b_{562} (dotted line); Fe^{3+}-cyt *c*-b_{562} (solid line); and Fe^{3+}-cyt c_{556} (dashed line).

Fe^{3+}-cyt *c*-b_{562}, $\epsilon_{415} = 0.148\ \mu M^{-1}\ cm^{-1}$; Fe^{2+}-cyt *c*-b_{562}, $\epsilon_{421} = 0.162\ \mu M^{-1}\ cm^{-1}$. Interestingly, the reduction potential of native *c*-b_{562} measured at a gold electrode modified with a cysteine-rich hexapeptide (KCTCCA) is identical with that reported for the wild-type protein ($E° = 189$ mV vs NHE) (*48*). This finding is somewhat surprising given the differences in electrostatic potential and covalent bonding at the heme in the two proteins. It is possible that the change in the His102 imidiazole angle compensates for differences in electrostatics and bonding, leading to an unchanged reduction potential.

Stability and Folding. GuHCl denaturation of the oxidized and reduced forms of cyt *c*-b_{562}, monitored by absorption,

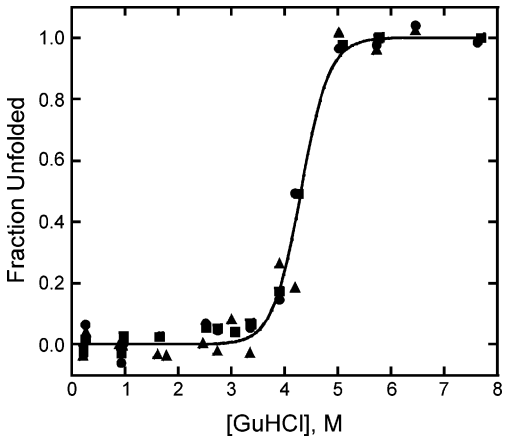

FIGURE 4: Denaturant-induced unfolding of Fe^{3+}-cyt *c*-b_{562} (pH 5) probed using absorption (circles), CD (squares), and Trp59 fluorescence (triangles) spectra. The solid line is a fit to a two-state folding model [$[GuHCl]_{1/2} = 4.3(1)$ M].

far-UV CD, and tryptophan fluorescence (Figure 4), is fully reversible. The oxidized protein has a stability maximum at pH 5, where the midpoint for unfolding ($[GuHCl]_{1/2}$) is 4.2 ± 0.05 M ($m = 10.1 \pm 0.1$ kJ mol^{-1} M^{-1}). The folding free energy change for cyt *c*-b_{562}, extrapolated to [GuHCl] = 0, is −42 ± 4 kJ mol^{-1}; this value is substantially greater than that estimated for the wild-type *b*-type protein (−30 kJ mol^{-1}) (*20*) and three times greater than that of the apoprotein (−13 kJ mol^{-1}) (*13*). The stability of the R98C mutant of cyt b_{562}, featuring a single *c*-type thioether link between the polypeptide and the protoporphyrin [−35.6(8) kJ mol^{-1}, $m = 8.4 \pm 0.2$ kJ mol^{-1} M^{-1}] (*20*), is greater than that of the *b*-type protein but less than that of the protein with two *c*-type linkages. It is important to note that the comparison between the proteins with one and two thioether links is complicated by the fact that the amino acid sequence of our cyt *c*-b_{562} differs in two locations (Y101C/K59W) from that of the R98C variant. Unfolding of Fe^{3+}-cyt *c*-b_{562} at pH 5 is accompanied by a large blue shift of the Soret maximum (folded, λ_{max} 415 nm; unfolded, λ_{max} 401 nm), consistent with the loss of axial ligation to Met7 and formation of a high-spin Fe^{3+}−heme center. The protein is less stable at pH 7, $[GuHCl]_{1/2} = 3.3 \pm 0.1$ M, and the small blue shift in Soret absorption upon denaturation (folded, λ_{max} 415 nm; unfolded, λ_{max} 408 nm) indicates that the heme remains low spin. Reasoning by analogy to cytochrome *c* (*49*, *50*), it is likely that Met7 is replaced by His63 as the axial heme ligand in the denatured protein.

To determine how changes in heme coordination affect the ensemble of unfolded protein structures, we examined fluorescence energy transfer kinetics between Trp59 (donor) and the heme group (acceptor) (*12*, *28*). In the folded Fe^{3+} protein, at pH 5 and 7, the Trp59 fluorescence decay kinetics are consistent with a narrow distribution of Trp59-to-heme distances (*r*) (Figure 5). Assuming that the Trp59 conformation in solution is the same as that found in the X-ray crystal structure, the FET kinetics suggest Trp−heme distances (pH 5, 21.5 Å; pH 7, 22.2 Å) that are in reasonable agreement with that determined crystallographically (18.9 Å).

Under denaturing conditions, the Trp59 fluorescence decay is slower and nonexponential, consistent with a heterogeneous ensemble of unfolded polypeptides. At pH 5, where protonated His63 does not coordinate to Fe^{3+}, the majority

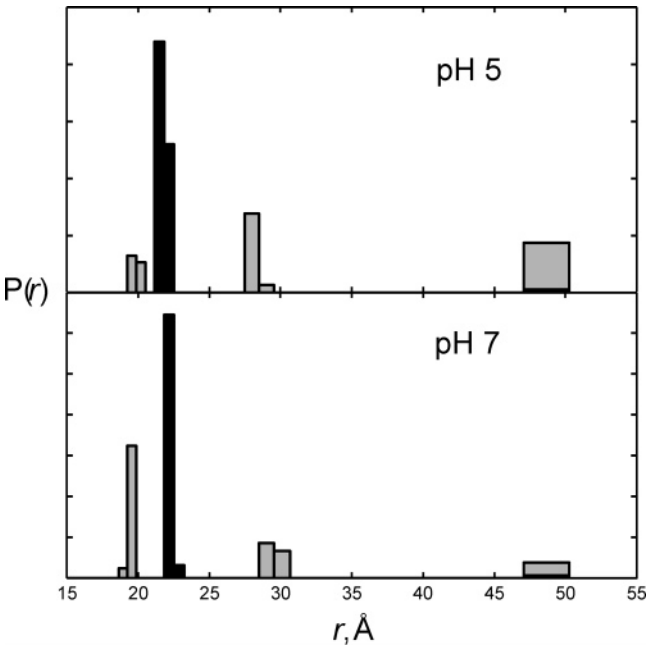

FIGURE 5: Distributions of Trp59−heme distances extracted from FET kinetics obtained in native (black) and denaturing (gray) environments at pH 5 and 7. The area of each bar is proportional to the probability of finding a tryptophan−heme in the distance range spanned by the width of the bar. The bars spanning 47−50 Å represent the probability of finding Trp−heme distances >47 Å.

of the population displays an extended conformation ($R_{DA} \geq 43$ Å). At pH 7, the unfolded protein retains a large fraction of a compact conformation ($R_{DA} \approx 19$ Å) attributable to His63−Fe misligation (Figure 5).

Refolding Kinetics. Owing to the reversibility of Fe^{3+}-cyt c-b_{562} denaturation, it is possible to study the refolding kinetics of this four-helix-bundle heme protein. The kinetics of stopped-flow triggered Fe^{3+}-cyt c-b_{562} refolding at pH 5 were probed by measurements of heme absorption at wavelengths characteristic of the denatured (398 nm) and native (418 nm) proteins. We find that formation of native Fe^{3+}-cyt c-b_{562} is biphasic. The rate constant for the faster phase varies with denaturant concentration and has an extrapolated rate constant of 4.2×10^2 s^{-1} at 0 M GuHCl. The rate of the slower phase is independent of denaturant concentration ($k_{obs} \approx 5$ s^{-1}). When refolding is monitored by Trp59 fluorescence, more than half of the signal amplitude is quenched during the mixing dead time (~5 ms) ($[GuHCl]_{final} = 0.3$ M, 90% loss of Trp59 fluorescence intensity; $[GuHCl]_{final} = 2$ M, 60%) (Figure 6). The remaining signal amplitude decays exponentially with a denaturant-dependent rate constant that corresponds to the faster phase observed using heme absorption spectroscopy (Figure 6).

The NMR structure of apocyt b_{562} suggests that the first three helices fold into a bundle with the final 10−12 residues (94−106) in rapid exchange among ordered conformations (*51*, *52*). Further, stability studies of the apoprotein are consistent with the presence of three cooperative folding units: helices 2 and 3 form the most stable unit; helices 1 and 4 represent independent folding units (*52*). The apoprotein folding rate constant ranges from ~10 s^{-1} at the midpoint denaturant concentration ($[urea]_{1/2} = 3.2 \pm 0.1$ M) to 2600 s^{-1} in the absence of denaturant (*13*). Using a redesigned

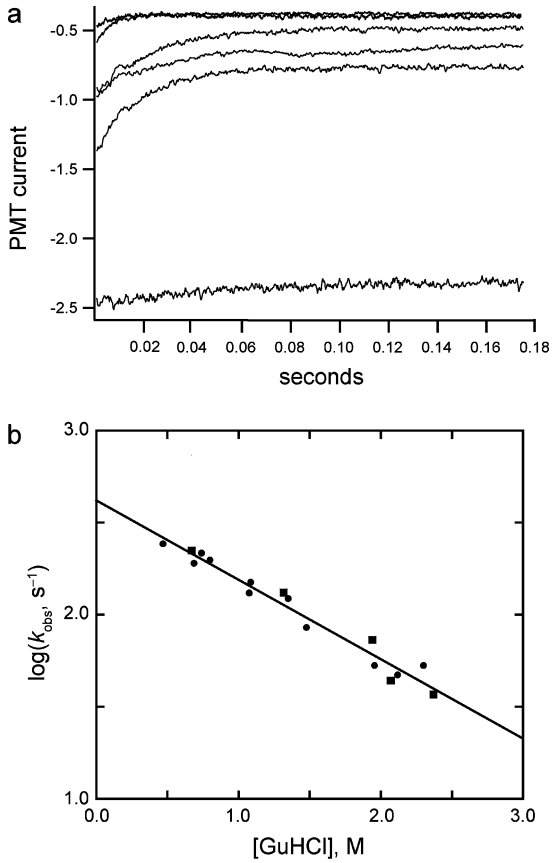

FIGURE 6: Refolding kinetics of cyt c-b_{562}. (a) Time dependence of tryptophan fluorescence intensity at different final GuHCl concentrations [[GuHCl] = 0.6, 1.4, 1.9, 2.1, 2.4, 7 M (upper to lower); [cyt c-b_{562}] = 10 μM]. (b) Dominant refolding rate constants for cyt c-b_{562} extracted from measurements of tryptophan fluorescence (squares) and Soret absorption (dots) measurements as functions of denaturant concentration.

apocyt b_{562} (Rd-apocyt b_{562}) and native state hydrogen exchange methods, Bai and co-workers have formulated a sequential folding mechanism (*53*) in which the rate-limiting step produces an intermediate (PUF1) with the N-terminal helix and part of the C-terminal helix unfolded. This species converts to a second intermediate (PUF2) in which just the N-terminal helix is unfolded. It is plausible that a similar sequential folding mechanism is operative in the holoprotein, cyt c-b_{562}. Covalent attachment of the porphyrin to the polypeptide in cyt c-b_{562} produces multiple refolding kinetics phases and an overall rate somewhat lower than that found for the apoprotein. Trp59 lies near the top of helix 3, close to the helix 2−3 loop. Formation of an intermediate analogous to PUF1, with helices 2 and 3 and the N-terminal part of helix 4 in near-native conformations, would bring Trp59 closer to the heme, producing the loss of fluorescence observed after the burst phase. Conversion of this species into an intermediate with a fully developed C-terminal helix (PUF2) involves positioning the heme adjacent to helices 2 and 3 and would be expected to produce a measurable change in heme absorbance as well as a further reduction in Trp59 fluorescence. The barrier to this PUF1−PUF2 conversion is likely to be greater in Fe^{3+}-cyt c-b_{562} than apocyt b_{562}, owing to the presence of the covalently attached porphyrin group. The final slow phase ($k_{obs} \approx 5$ s^{-1}) observed by absorption spectroscopy could involve formation of the native heme coordination environment [Fe−S(Met7)].

The native *b*-type ferric protein has been suggested to follow a sequential folding pathway in which rapid apoprotein folding precedes heme binding (*13*), leading to relatively slow formation of the native structure. The *c*-type linkage in cyt *c*-b_{562} clearly leads to more efficient delivery of the heme into the preformed helical bundle. Judged by the formation of native heme environment, the refolding of Fe^{3+}-cyt *c*-b_{562} appears to be considerably slower than that of the reduced protein ($\geq 10^4$ s^{-1}) (*25*). The fast folding of reduced cyt *c*-b_{562} was attributed to formation of a persistent native contact between S(Met7) and the Fe^{2+}−heme center during refolding. The early formation of this native contact would create a folding sequence different from that of Fe^{3+}-cyt *c*-b_{562}. Owing to S(Met7)−Fe^{2+} ligation, the N- and C-terminal regions of the polypeptide will be held together such that bundle formation in helices 2−3 could produce a protein with a near-native structure.

Finally, it is of interest to contrast the refolding kinetics of Fe^{3+}-cyt *c*-b_{562} with those of Fe^{3+}-cyt *c*′, a much slower folding protein (*11*, *12*). Although the two proteins have quite similar folds, the amino acid sequence of cyt *c*′ has a lower helix propensity than cyt b_{562}. It is possible that the rapid bundle formation in helices 2−3 that produces efficient cyt *c*-b_{562} folding does not lead the way in Fe^{3+}-cyt *c*′.

ACKNOWLEDGMENT

We thank Dr. J. C. Lee for helpful comments and suggestions and Prof. D. C. Rees for the use of X-ray facilities.

REFERENCES

1. Plaxco, K. W., Simons, K. T., and Baker, D. (1998) Contact Order, Transition State Placement and the Refolding Rates of Single Domain Proteins, *J. Mol. Biol. 277*, 985−994.
2. Plaxco, K. W., Simons, K. T., Ruczinski, I., and Baker, D. (2000) Topology, Stability, Sequence, and Length: Defining the Determinants of Two-State Protein Folding Kinetics, *Biochemistry 39*, 11177−11183.
3. Shortle, D., and Ackerman, M. S. (2001) Persistence of Native-Like Topology in a Denatured Protein in 8 M Urea, *Science 293*, 487−489.
4. Zarrine-Afsar, A., Larson, S. M., and Davidson, A. R. (2005) The Family Feud: Do Proteins with Similar Structures Fold via the Same Pathway?, *Curr. Opin. Struct. Biol. 15*, 42−49.
5. Friel, C. T., Capaldi, A. P., and Radford, S. E. (2003) Structural Analysis of the Rate-limiting Transition States in the Folding of Im7 and Im9: Similarities and Differences in the Folding of Homologous Proteins, *J. Mol. Biol. 326*, 293−305.
6. Rozwarski, D. A., Gronenborn, A. M., Clore, G. M., Bazan, J. F., Bohm, A., Wlodawer, A., Hatada, M., and Karplus, P. A. (1994) Structural Comparisons among the Short-Chain Helical Cytokines, *Structure 2*, 159−173.
7. Wilson, C., Mau, T., Weisgraber, K. H., Wardell, M. R., Mahley, R. W., and Agard, D. A. (1994) Salt Bridge Relay Triggers Defective LDL Receptor Binding by a Mutant Apolipoprotein, *Structure 2*, 713−718.
8. de Vos, A. M., Ultsch, M., and Kossiakoff, A. A. (1992) Human Growth Hormone and Extracellular Domain of its Receptor: Crystal Structure of the Complex, *Science 255*, 306−312.
9. Tonello, F., Dundon, W. G., Satin, B., Molinari, M., Tognon, G., Grandi, G., Del Giudice, G., Rappuoli, R., and Montecucco, C. (1999) The *Helicobacter pylori* Neutrophil-Activating Protein is an Iron-Binding Protein with Dodecameric Structure, *Mol. Microbiol. 34*, 238−246.
10. Wittung-Stafshede, P., Lee, J. C., Winkler, J. R., and Gray, H. B. (1999) Cytochrome b_{562} Folding Triggered by Electron Transfer: Approaching the Speed Limit for Formation of a Four-Helix-Bundle Protein, *Proc. Natl. Acad. Sci. U.S.A. 96*, 6587−6590.
11. Lee, J. C., Gray, H. B., and Winkler, J. R. (2001) Cytochrome *c*′ Folding Triggered by Electron Transfer: Fast and Slow Formation of Four-Helix Bundles, *Proc. Natl. Acad. Sci. U.S.A. 98*, 7760−7764.
12. Lee, J. C., Engman, K. C., Tezcan, F. A., Gray, H. B., and Winkler, J. R. (2002) Structural Features of Cytochrome *c*′ Folding Intermediates Revealed by Fluorescence Energy-Transfer Kinetics, *Proc. Natl. Acad. Sci. U.S.A. 99*, 14778−14782.
13. Garcia, P., Bruix, M., Rico, M., Ciofi-Baffoni, Banci, L., Shastry, M. C. R., Roder, H., Woodyear, T. D., Johnson, C. M., Fersht, A. R., and Barker, P. D. (2005) Effects of Heme on the Structure of the Denatured State and Folding Kinetics of Cytochrome b_{562}, *J. Mol. Biol. 346*, 331−344.
14. Shibata, N., Iba, S., Misaki, S., Meyer, T. E., Bartsch, R. G., Cusanovich, M. A., Morimoto, Y., Higuchi, Y., and Yasuoka, N. (1998) Basis for Monomer Stabilization in *Rhodopseudomonas palustris* Cytochrome *c*′ Derived from the Crystal Structure, *J. Mol. Biol. 284*, 751−760.
15. Bertini, I., Faraone-Mennella, J., Gray, H. B., Luchinat, C., Parigi, G., and Winkler, J. R. (2004) NMR-Validated Structural Model for Oxidized *Rhodopseudomonas palustris* Cytochrome c_{556}, *J. Biol. Inorg. Chem. 9*, 224−230.
16. Arnesano, F., Banci, L., Bertini, I., Faraone-Mennella, J., Rosato, A., Barker, P. D., and Fersht, A. R. (1999) The Solution Structure of Oxidized *Escherichia coli* Cytochrome b_{562}, *Biochemistry 38*, 8657−8670.
17. Stevens, J. M., Daltrop, O., Allen, J. W. A., and Ferguson, S. J. (2004) *c*-Type Cytochrome Formation: Chemical and Biological Enigmas, *Acc. Chem. Res. 37*, 999−1007.
18. Barker, P. D., Nerou, E. P., Freund, S. M. V., and Fearnley, I. M. (1995) Conversion of Cytochrome b_{562} to *c*-Type Cytochromes, *Biochemistry 34*, 15191−15203.
19. Rice, J. K., Fearnley, I. M., and Barker, P. D. (1999) Coupled Oxidation of Heme Covalently Attached to Cyctochrome b_{562} Yields a Novel Biliprotein, *Biochemistry 38*, 16847−16856.
20. Arnesano, F., Banci, L., Bertini, I., Ciofi-Baffoni, S., de Lumley Woodyear, T., Johnson, C. M., and Barker, P. D. (2000) Structural Consequences of *b*- to *c*-Type Heme Conversion in Oxidized *Escherichia coli* Cytochrome b_{562}, *Biochemistry 39*, 1499−1514.
21. Arslan, E., Schulz, H., Zufferey, R., Künzler, P., and Thöny-Meyer, L. (1998) Overproduction of the *Bradyrhizobium japonicum c*-Type Cytochrome Subunits of the cbb_3 Oxidase in *Escherichia coli*, *Biochem. Biophys. Res. Commun. 251*, 744−747.
22. Allen, J. W. A., Barker, P. D., and Ferguson, S. J. (2003) A Cytochrome b_{562} Variant with a *c*-Type Cytochrome CXXCH Heme-Binding Motif as a Probe of the *Escherichia coli* Cytochrome *c* Maturation System, *J. Biol. Chem. 278*, 52075−52083.
23. Allen, J. W. A., and Ferguson, S. J. (2006) The *Escherichia coli* Cytochrome *c* Maturation (Ccm) Apparatus Can Mature Cytochromes with an Extra Cysteine within or adjacent to the CXXCH Motif, *Biochem. Soc. Trans. 34*, 91−93.
24. Nikkila, H., Gennis, R. B., and Sligar, S. G. (1991) Cloning and Expression of the Gene Encoding the Soluble Cytochrome b_{562} of *Escherichia coli*, *Eur. J. Biochem. 202*, 309−313.
25. Faraone-Mennella, J., Gray, H. B., and Winkler, J. R. (2005) Early Events in the Folding of Four-Helix-Bundle Heme Proteins, *Proc. Natl. Acad. Sci. U.S.A. 102*, 6315−6319.
26. McGuirl, M. A., Lee, J. C., Lyubovitsky, J. G., Thanyakoop, C., Richards, J. H., Gray, H. B., and Winkler, J. R. (2003) Cloning, Heterologous Expression, and Characterization of Recombinant Class II Cytochromes from *Rhodopseudomonas palustris*, *Biochim. Biophys. Acta 1619*, 23−28.
27. Nozaki, Y. (1972) The Preparation of Guanidine Hydrochloride, *Methods Enzymol. 26*, 43−50.
28. Lee, J. C., Langen, R., Hummel, P. A., Gray, H. B., and Winkler, J. R. (2004) α-Synuclein Structures from Fluorescence Energy-Transfer Kinetics: Implications for the Role of the Protein in Parkinson's Disease, *Proc. Natl. Acad. Sci. U.S.A. 101*, 16466−16471.
29. Förster, T. (1948) Zwischenmolekulare Energiewanderung und Fluoreszenz, *Ann. Phys. (Leipzig) 2*, 55−75.
30. Gryczynski, Z., Lubkowski, J., and Bucci, E. (1997) Intrinsic Fluorescence of Hemoglobins and Myoglobins, *Methods Enzymol. 278*, 538−569.
31. Otwinowski, Z., and Minor, W. (1997) Processing of X-ray Diffraction Data Collected in Oscillation Mode, *Methods Enzymol. 276*, 307−326.
32. Bailey, S. (1994) The CCP4 Suite—Programs for Protein Crystallography, *Acta Crystallogr. D 50*, 760−763.

33. Lederer, F., Glatigny, A., Bethge, P. H., Bellamy, H. D., and Mathews, F. S. (1981) Improvement of the 2.5 Å Resolution Model of Cytochrome b_{562} by Redetermining the Primary Structure and Using Molecular Graphics, *J. Mol. Biol. 148*, 427−448.
34. Brünger, A. T., Adams, P. D., Clore, G. M., DeLano, W. L., Gros, P., Grosse-Kunstleve, R. W., Jiang, J. S., Kuszewski, J., Nilges, M., Pannu, N. S., Read, R. J., Rice, L. M., Simonson, T., and Warren, G. L. (1998) Crystallography & NMR System: A New Software Suite for Macromolecular Structure Determination, *Acta Crystallogr. D 54*, 905−921.
35. McRee, D. E. (1999) XtalView Xfit−A Versatile Program for Manipulating Atomic Coordinates and Electron Density, *J. Struct. Biol. 125*, 156−165.
36. Laskowski, R. A., Macarthur, M. W., Moss, D. S., and Thornton, J. M. (1993) PROCHECK−A Program to Check the Stereochemical Quality of Protein Structures, *J. Appl. Crystallogr. 26*, 283−291.
37. Pollock, W. B. R., Rosell, F. I., Twitchett, M. B., Dumont, M. E., and Mauk, A. G. (1998) Bacterial Expression of a Mitochondrial Cytochrome *c*. Trimethylation of Lys72 in Yeast *iso*-1-Cytochrome *c* and the Alkaline Conformational Transition, *Biochemistry 37*, 6124−6131.
38. Rumbley, J. N., Hoang, L., and Englander, S. W. (2002) Recombinant Equine Cytochrome *c* in *Escherichia coli*: High-Level Expression, Characterization, and Folding and Assembly Mutants, *Biochemistry 41*, 13894−13901.
39. Sanders, C., and Lill, H. (2000) Expression of Prokaryotic and Eukaryotic Cytochromes *c* in *Escherichia coli*, *Biochim. Biophys. Acta Bioenerg. 1459*, 131−138.
40. Thöny-Meyer, L. (2002) Cytochrome *c* Maturation: a Complex Pathway for a Simple Task?, *Biochem. Soc. Trans. 30*, 633−638.
41. Kranz, R., Lill, R., Goldman, B., Bonnard, G., and Merchant, S. (1998) Molecular Mechanisms of Cytochrome *c* Biogenesis: Three Distinct Systems, *Mol. Microbiol. 29*, 383−396.
42. Braun, M., and Thöny-Meyer, L. (2004) Biosynthesis of Artificial Microperoxidases by Exploiting the Secretion and Cytochrome *c* Maturation Apparatuses of *Escherichia coli*, *Proc. Natl. Acad. Sci. U.S.A. 101*, 12830−12835.
43. Fee, J. A., Chen, Y., Todaro, T. R., Bren, K. L., Patel, K. M., Hill, M. G., Ester, G.-M., Loehr, T. M., Ai, J., Thöny-Meyer, L., Williams, P. A., Stura, E., Sridhar, V., and McRee, D. E. (2000) Integrity of *Thermus thermophilus* Cytochrome c_{552} Synthesized by *Escherichia coli* Cells Expressing the Host-Specific Cytochrome *c* Maturation Genes, *ccmABCDEFGH*: Biochemical, Spectral, and Structural Characterization of the Recombinant Proteins, *Protein Sci. 9*, 2074−2084.
44. Gallivan, J. P., and Dougherty, D. A. (2000) A Computational Study of Cation-Pi Interactions vs Salt Bridges in Aqueous Media: Implications for Protein Engineering, *J. Am. Chem. Soc. 122*, 870−874.
45. Sakurai, K., Mizuno, T., Hiroaki, H., Gohda, K., Oku, J., and Tanaka, T. (2005) High Thermal Stability Imparted by a Designed Tandem Arg-Trp Stretch in an Alpha-Helical Coiled Coil, *Angew. Chem., Int. Ed. 44*, 6180−6183.
46. Waters, M. L. (2004) Aromatic Interactions in Peptides: Impact on Structure and Function, *Biopolymers 76*, 435−445.
47. Berry, E. A., and Trumpower, B. L. (1987) Simultaneous Determination of Hemes *a*, *b*, and *c* from Pyridine Hemochrome Spectra, *Anal. Biochem. 161*, 1−15.
48. Barker, P. D., Butler, J. L., de Oliveira, P., Hill, H. A. O., and Hunt, N. I. (1996) Direct Electrochemical Studies of Cytochromes b_{562}, *Inorg. Chim. Acta 252*, 71−77.
49. Babul, J., and Stellwagen, E. (1971) The Existence of Heme-Protein Coordinate-Covalent Bonds in Denaturing Solvents, *Biopolymers 10*, 2359−2361.
50. Colón, W., Wakem, L. P., Sherman, F., and Roder, H. (1997) Identification of the Predominant Non-Native Histidine Ligand in Unfolded Cytochrome *c*, *Biochemistry 36*, 12535−12541.
51. Feng, Y., Wand, A. J., and Sligar, S. G. (1991) ^{1}H and ^{15}N NMR Resonance Assignments and Preliminary Structural Characterization of *Escherichia coli* Apocytochrome b_{562}, *Biochemistry 30*, 7711−7717.
52. D'Amelio, N., Bonvin, A. M. J. J., Czisch, M., Barker, P., and Kaptein, R. (2002) The C Terminus of Apocytochrome b_{562} Undergoes Fast Motions and Slow Exchange among Ordered Conformations Resembling the Folded State, *Biochemistry 41*, 5505−5514.
53. Feng, H., Zhou, Z., and Bai, Y. (2005) A Protein Folding Pathway with Multiple Folding Intermediates at Atomic Resolution, *Proc. Natl. Acad. Sci. U.S.A. 102*, 5026−5031.

BI060242X